Elementary excitations in superfluid ^{3}He-^{4}He mixtures: Pressure and temperature dependence

B. Fåk*
Department of Neutron Research, Uppsala University, 611 82 Nyköping, Sweden

K. Guckelsberger, M. Körfer,† and R. Scherm
Physikalisch-Technische Bundesanstalt, 3300 Braunschweig, Federal Republic of Germany

A. J. Dianoux
Institut Laue-Langevin, 38042 Grenoble, France
(Received 10 October 1989)

The neutron-scattering function for dilute mixtures of ^{3}He (1% and 5%) in superfluid ^{4}He at pressures of 0, 10, and 18 bars and temperatures in the range from 0.07 to 1.5 K has been determined for wave vectors between 0.4 and 2.2 Å^{-1}. This is the first such measurement for ^{3}He-^{4}He mixtures at temperatures below the Fermi temperature. The line shape of the ^{3}He particle-hole excitation is well described by a nearly-free-Fermi-gas model at all temperatures. The ^{3}He quasiparticle spectrum is derived for wave vectors in the range $0.9 < Q < 1.7$ Å^{-1}. The results deviate from the quadratic Landau-Pomeranchuk spectrum and are in good agreement with thermodynamical measurements. No rotonlike minimum is observed. We find strong indications of a crossover between the ^{3}He particle-hole band and the ^{4}He roton excitation. The pressure and temperature dependence of the shift and broadening of the ^{4}He phonon-roton peak is derived. The main features are reproduced in a simple model for Landau damping.

I. INTRODUCTION

Liquid ^{4}He, a model system for a Bose liquid, has been extensively studied by neutron scattering in the past.[1] The spectrum of elementary excitations is well known for a large range of wave vectors and for many pressures and temperatures. For wave vectors less than 2 Å^{-1} (energies less than 15 K), the excitation spectrum is dominated by collective density fluctuations, the phonon-roton (ph-r) excitation, characterized by a single dispersion curve. The dispersion is nearly linear for wave vectors less than 0.6 Å^{-1}, with a small anomalous contribution. At wave vectors around 1.1 Å^{-1} the dispersion has a maximum (the so-called maxon), followed by the roton minimum at 1.9 Å^{-1}. In addition, the ^{4}He spectrum exhibits multiphonon excitations at higher energies. For details we refer to the recent review by Glyde and Svensson.[1]

Liquid ^{3}He, which has a nuclear spin of $\frac{1}{2}$, is a model system for a Fermi liquid and is the only *neutral* Fermi liquid experimentally accessible. Because of the large neutron-absorption cross section of ^{3}He, neutron-scattering experiments are difficult. Nevertheless, in recent years such measurements have become feasible and experimental results are now available for several pressures and temperatures.[1,2] The excitation spectrum consists of a band of particle-hole (p-h) excitations at energies lower than expected from a free Fermi gas, indicating a quasiparticle effective mass of about 3 times the bare mass. At small wave vectors, spin fluctuations in the p-h continuum enhance the low-energy part of the spectrum, sometimes referred to as the paramagnon resonance. In addition to the p-h band, ^{3}He also sustains collective density fluctuations, the zero-sound mode, with striking resemblance to ph-r excitations in ^{4}He.[3] Multipair excitations and possibly multiphonons are also present in the excitation spectrum of liquid ^{3}He. A comprehensive summary of these results is found in Ref. 1. For the most recent experimental results we refer to the papers by Scherm *et al.*,[2,3] and for recent theoretical results we refer to the papers by Hess and Pines,[4] Holas and Singwi,[5] and Dalfovo and Stringari.[6]

At low temperatures the thermal properties of dilute mixtures of ^{3}He in superfluid ^{4}He are well described by treating the ^{3}He subsystem as a weakly interacting Fermi gas. The excitation spectrum has two branches: Fermi-gas-like p-h excitations arising from ^{3}He, and a well-defined collective phonon-roton excitation, mainly from ^{4}He. In dilute mixtures the effective ^{3}He-^{3}He interaction is too weak to sustain a zero-sound excitation of its own. The influence of ^{3}He impurities on the ^{4}He excitations is also small, but sufficient to slightly shift and broaden the ph-r peak. In the past, neutron-inelastic-scattering experiments on mixtures have been performed by two groups: Rowe *et al.*[7] studied a 5% mixture at saturated vapor pressure (SVP) at a temperature of 1.6 K, while the study by Hilton *et al.*[8] included mixtures of 6%, 12%, and 25% at SVP for temperatures between 0.6 and 1.5 K. Both groups report broadening as well as a small shift of the ph-r excitation, although they disagree on the sign of the shift.

Hilton *et al.* could explain the main contribution to the observed energy shift by a strikingly simple model.

They suggest that the wave vector $Q_{\rm mix}$ in the mixture data should be rescaled relative to the wave vector Q_4 in the pure ^{4}He data by the number densities n_4 and $n_{\rm mix}$, according to the formula

$$Q_{\rm mix}=Q_4(n_{\rm mix}/n_4)^{1/3} . \quad (1)$$

This takes into account the fact that, at a given pressure, the molar volume of the mixture is larger than that of pure ^{4}He. The underlying reason is the larger zero-point motion of the ^{3}He atoms. This *ad hoc* model, hereafter referred to as density scaling, was later put on firm theoretical ground by Lücke *et al.*[9] and by Hsu *et al.*[10] Earlier calculations[11–16] had neglected this effect, which in fact gives the dominant contribution to the energy shift. To focus the study on more fundamental mechanisms for the shift, such as mode-mode coupling and renormalization due to scattering, we measured pure ^{4}He and the mixture at the same number density. In practice, this means that the mixture is measured at a pressure p slightly higher than the pressure p' of ^{4}He, typically of the order of 1 bar. The shift at constant density, at temperature T, and ^{3}He concentration x_3, is thus defined as the difference in excitation energy between the mixture and low-temperature pure ^{4}He, i.e.,

$$\delta\omega=\omega(p,x_3,T)-\omega(p',x_3=0,T\to 0) . \quad (2)$$

In the experiment by Hilton *et al.* the p-h excitations were observed at a temperature well above the Fermi temperature T_F, which for a 5% mixture at SVP is about 0.3 K. At this temperature the p-h excitations are thermally broadened. The present study, in which the measurements were extended down to temperatures of 0.07 K, therefore represents the first measurement below T_F. The p-h excitations are, in this case, well defined and we could study the broadening and line shape as a function of temperature. The experiment also gives directly the quasiparticle spectrum for intermediate wave vectors $0.9<Q<1.7$ Å^{-1}.

This paper is organized as follows. Section II describes the experimental details. The results for the p-h excitations are presented in Sec. III together with a discussion on the possible crossover between the p-h band and the ph-r mode. In Sec. IV the results for the ph-r excitation are given, and they are compared with theoretical calculations in Sec. V. The main results and the conclusions are summarized in Sec. VI.

II. MEASUREMENTS

A. Thermal neutron scattering

In an neutron-inelastic-scattering experiment the quantity measured is the double-differential cross section which, for a mixture of liquid ^{3}He-^{4}He, is given by[1,17]

$$\frac{d^2\sigma}{d\Omega\,dE_1}=\frac{k_1}{k_0}\frac{1}{4\pi\hbar}\{\sigma_4^c(1-x_3)S_{44}^c(Q,\omega)+\sigma_3^c x_3 S_{33}^c(Q,\omega)+\sigma_3^i x_3 S_{33}^I(Q,\omega)+\sigma_{34}^c[x_3(1-x_3)]^{1/2}S_{34}^c(Q,\omega)\}$$
$$\equiv\frac{k_1}{k_0}\frac{1}{4\pi\hbar}[\sigma_4^c(1-x_3)+(\sigma_3^c+\sigma_3^i)x_3]\hat{S}(Q,\omega) , \quad (3)$$

where x_3 is the molar concentration of ^{3}He. The energy and wave-vector transfer in the scattering process is

$$\hbar\omega=E_0-E_1 ,$$
$$\mathbf{Q}=\mathbf{k}_0-\mathbf{k}_1 , \quad (4)$$

where the subscript 0 (1) denotes the initial (final) state of the neutron. The cross sections calculated from the scattering lengths given by Sears[18] are (in units of barns) $\sigma_4^c=1.34$, $\sigma_3^c=4.42$, $\sigma_3^i=1.19$, and $\sigma_{34}^c=4\pi 2\,\mathrm{Re}\{b_3b_4\}=4.70$. The coherent-scattering function, which describes number-density correlations, is given by

$$S_{dd'}^c(Q,\omega)=\frac{1}{(N_dN_{d'})^{1/2}}\frac{1}{2\pi}\sum_{\substack{j\in d\\ j'\in d'}}\int_{-\infty}^{\infty}\langle\exp[-i\mathbf{Q}\cdot\mathbf{R}_j(0)]\exp[i\mathbf{Q}\cdot\mathbf{R}_{j'}(t)]\rangle\exp(-i\omega t)dt , \quad (5)$$

where d and d' denote different isotopes. N_d is the number of atoms of type d and $\mathbf{R}_j$ is the position of atom j. The angular brackets denote thermal averages. Correlations in the spin density (of one isotope) is measured by

$$S_{dd}^I(Q,\omega)=\frac{1}{N_d}\frac{1}{2\pi}\sum_{\substack{j\in d\\ j'\in d}}\int_{-\infty}^{\infty}\langle\mathbf{I}_j\cdot\mathbf{I}_{j'}\exp[-i\mathbf{Q}\cdot\mathbf{R}_j(0)]\exp[i\mathbf{Q}\cdot\mathbf{R}_{j'}(t)]\rangle\frac{1}{I(I+1)}\exp(-i\omega t)dt , \quad (6)$$

where $\mathbf{I}_j$ is the spin of nucleus j. In the absence of spin correlations, Eq. (6) reduces to the incoherent- (self-correlation) scattering function

$$S_d^i(Q,\omega)=\frac{1}{N_d}\frac{1}{2\pi}\sum_{j\in d}\int_{-\infty}^{\infty}\langle\exp[-i\mathbf{Q}\cdot\mathbf{R}_j(0)]\exp[i\mathbf{Q}\cdot\mathbf{R}_j(t)]\rangle\exp(-i\omega t)dt . \quad (7)$$

Each of the partial scattering functions independently satisfies the f-sum rule[17]

$$\int S^c_{dd'}(Q,\omega)\hbar\omega\, d\omega = \frac{\hbar^2 Q^2}{2m_d}\delta_{dd'} , \tag{8a}$$

$$\int S^i_d(Q,\omega)\hbar\omega\, d\omega = \frac{\hbar^2 Q^2}{2m_d} . \tag{8b}$$

The total scattering function $S(Q,\omega)$ in a multicomponent system is not uniquely normalized. We define it as $\hat{S}(Q,\omega)$ in Eq. (3). The coherent cross term S_{34} describes correlations between ^{3}He and ^{4}He atoms.[9,19] We assume that this term remains small for small concentrations. This allows us to identify peaks in $\hat{S}(Q,\omega)$ with either ^{3}He or ^{4}He excitations. We define the total scattering function for ^{3}He as

$$\hat{S}_3(Q,\omega) = \left[1+\frac{\sigma^c_4(1-x_3)}{(\sigma^c_3+\sigma^i_3)x_3}\right]\hat{S}(Q,\omega)$$
$$= \frac{\sigma^c_3 S^c_{33}(Q,\omega)+\sigma^i_3 S^I_{33}(Q,\omega)}{\sigma^c_3+\sigma^i_3} . \tag{9}$$

If we assume, in view of the weak ^{3}He-^{3}He interaction, that $S^c_{33}(Q,\omega)=S^I_{33}(Q,\omega)=S^i_{33}(Q,\omega)$, then $\hat{S}_3(Q,\omega)$ equals $S^c_{33}(Q,\omega)$ with the definition of Eq. (9), provided that $S_{34}=0$. For the discussion of ph-r excitations, we define $\hat{S}_4(Q,\omega)$ from Eq. (3) in a similar way.

B. Data acquisition

The measurements were made using the IN6 time-of-flight spectrometer[20] at the high-flux reactor at the Institut Laue-Langevin in Grenoble. Three vertically focusing pyrolytic-graphite monochromators, placed after each other in the neutron guide on the cold source, select three slightly shifted wavelength bands from the incident beam, which are then time focused by a straight-slit Fermi chopper. A 12-cm-long liquid-nitrogen-cooled polycrystalline-Be filter in the incident beam suppresses higher-order contamination to less than 1×10^{-4} of the first-order intensity. The incident energy was 44.3 K (3.82 meV) which corresponds to a wavelength of 4.63 Å. This wavelength is long enough to avoid Bragg scattering from extraneous materials in the beam, and small enough to allow wave vectors just above the roton minimum to be observed. Neutrons were recorded in detectors covering 4% of the total solid angle at scattering angles between 17° and 114°, which corresponds to wave-vector transfers for elastic scattering of $0.4<Q<2.2$ Å^{-1}. Energy transfers between -20 K and 35 K were recorded. Cd baffles in the incident flight path limited the beam area to 23×50 mm^2. In conjunction with an oscillating radial collimator in the scattered beam, this assured that only neutrons scattered by the sample and the sample container could reach the detectors directly. A more complete description of the experimental setup is found in Ref. 21.

A new sample container (Fig. 1) was made for this experiment, in a design similar to that used in a previous experiment[2] on pure ^{3}He, but with a slab geometry. A thin sample is required in order to minimize resolution broadening in pure ^{4}He. However, this makes background subtraction more difficult as neutrons elastically scattered by the Cd covering at the rear wall of the container contribute in the case of ^{4}He and empty-container measurements, but not in the mixture measurements. This scattering is as intense as the scattering from ^{3}He. The angle of 15.9° between the incident beam and the sample surface was accurately measured in the cold cryostat by a special device that scattered neutrons at 55°. This device was mounted below the sample, together with a 0.5-mm-thick vanadium sheet in a geometry identical to that of the sample. By raising and lowering the cryostat, scattering from the vanadium was measured between sample measurements in order to monitor changes in the detector efficiencies during the experiment. No such changes were observed, however. The scattering from vanadium was also used for absolute normalization of the data.

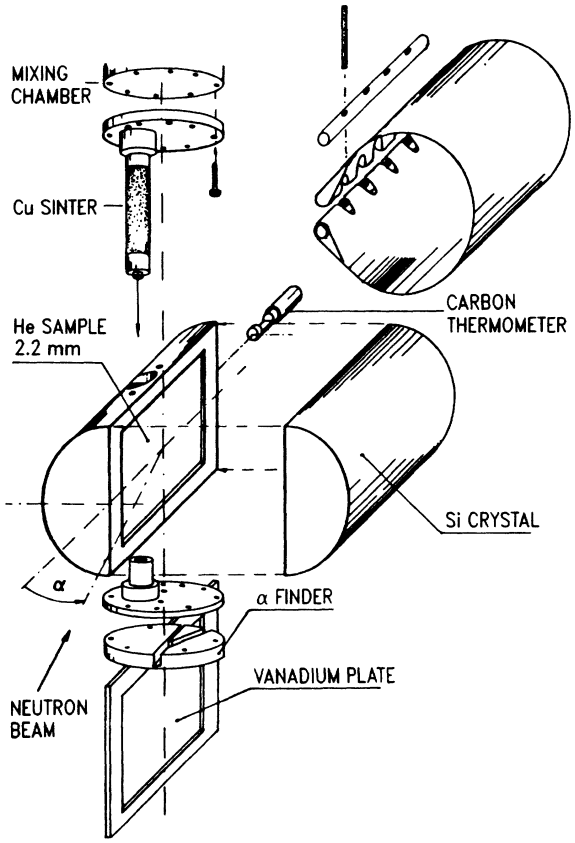

FIG. 1. Exploded view of the high-pressure-sample container with direction (α) finder and vanadium slab for normalization. The sample chamber is 64-mm high and 98-mm long.

The sample was cooled in an Oxford-Instruments dilution refrigerator. In a previous experiment[2] on pure ^{3}He the lowest sample temperature achieved was 120 mK. In the present experiment, a Cu sinter on the cold finger that connected the mixing chamber of the refrigerator with the sample improved the thermal contact. Despite this, beam heating increased the sample temperature from 30 to 70 mK. The temperature was measured by a

TABLE I. Experimental parameters (^{3}He concentration, pressure, and temperature) of all 26 measurements performed. The Fermi temperature and wave vector are given for convenience.

x_3 (%)	p (bar)	Temperatures (K)						T_F (K)	k_F (Å^{-1})
0	0.0	0.07				0.95	1.50		
0	4.9	0.07							
0	10.0	0.07				0.90	1.50		
0	18.0	0.07				0.90	1.50		
1.0	0.1	0.07						0.12	0.186
0.9	10.3	0.07						0.11	0.185
0.8	18.2	0.07						0.10	0.181
4.7	1.6	0.07			0.60	0.90	1.50	0.35	0.313
4.5	12.7	0.07	0.15	0.30	0.60	0.90	1.50	0.32	0.318
4.1	19.5	0.07				0.90	1.50	0.29	0.312

carbon resistor immersed in the liquid and by germanium and carbon resistors on various parts of the cold finger and on the mixing chamber. The temperature was controlled to better than 5 mK by two heaters, one on the mixing chamber and one on the sample.

Sixteen measurements on mixtures at different pressures, concentrations, and temperatures, 10–24 h each were performed, as well as ten measurements on pure ^{4}He at corresponding pressures and temperatures (2 h each), as shown in Table I. Scattering from the empty container was measured both before and after the sample runs at temperatures less than 0.1 K and for 29 h in total. In order to remove the helium sample completely, the container was pumped for several hours at temperatures up to 15 K.

After normalization to equal beam-monitor counts the empty-container scattering was subtracted from the full-container scattering. Due to the scattering from the rear wall this gives a false negative elastic peak. This has no influence on the ph-r peak, but affects the particle-hole (p-h) spectrum at low energies. Corrections were made for self-absorption in the sample, attenuation in the container window, and energy dependence of the detector efficiencies; the data were transformed from time of flight to energy-transfer representation. After absolute normalization using the vanadium data, the scattering function at constant angle $\hat{S}(\phi,\omega)$ was obtained. $\hat{S}(\phi,\omega)$ is shown in Fig. 2 for a few selected angles. The scattering function at constant Q, $\hat{S}(Q,\omega)$, shown in Fig. 3, was obtained by regrouping the data. Since data at 81 individual scattering angles were available, only a modest smoothing was involved. We used the constant-Q data to analyze the p-h excitations, since the energy width of the band is rather large. The constant-angle data were used for the sharp ph-r excitations, however. This avoids errors due to irregularities in the line shape, which are sometimes caused by regrouping routines. Full details of the data reduction will be given elsewhere.[22]

The final experimental results, $\hat{S}(\phi,\omega)$ and $\hat{S}(Q,\omega)$, represent convolutions of the actual scattering functions with the instrumental-resolution function. The contribution from multiple scattering is negligible because of the sample geometry.[23,24]

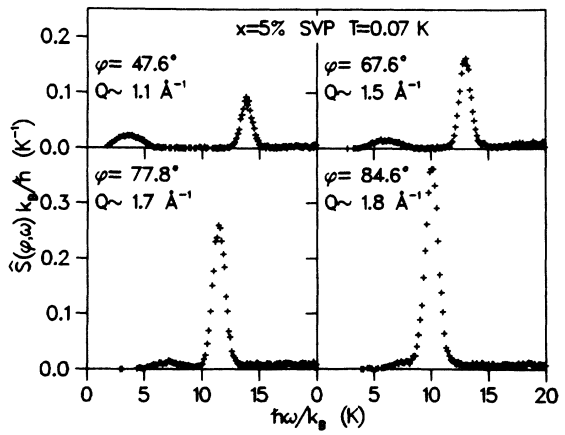

FIG. 2. Neutron-scattering function $\hat{S}(\phi,\omega)$ for selected angles. With increasing wave vector the low-energy particle-hole peak becomes weaker as it approaches the large phonon-roton peak.

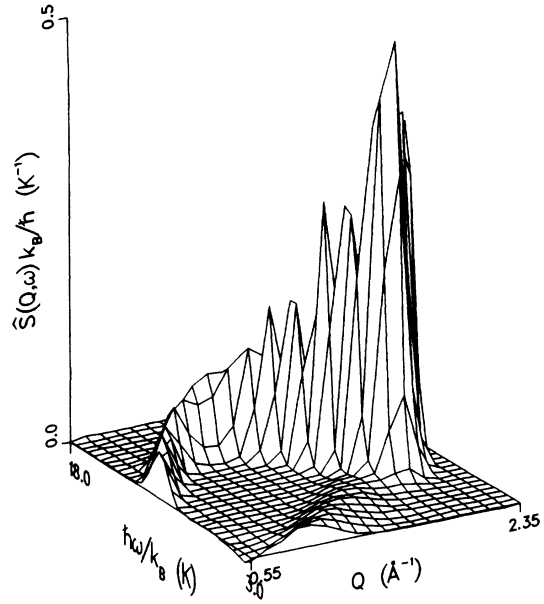

FIG. 3. Three-dimensional plot of the neutron-scattering function $\hat{S}(Q,\omega)$ for $x_3=5\%$ at SVP and $T=0.07$ K. The sawtooth "ridge" of the phonon-roton excitation is an artifact of the plotting routine and does not affect the data analysis.

C. Pressure and concentration variations

Due to pressure drifts and depletion of ^{3}He in the mixtures, the number density of the samples could only be controlled to within 1%, leading to a shift of the ph-r excitation. However, since the concentration, the average pressure, and the pressure variations could be determined for each measurement, we can correct for this effect, as described below.

The mixtures were prepared by condensing known amounts of ^{3}He and ^{4}He consecutively through a thin capillary that passes through the liquid-^{4}He bath to the sample container. The cold volume was sealed off from the large room-temperature volume with a valve on top of the cryostat. The sample pressure was regularly measured by opening this room-temperature valve to a high-precision Bourdon gauge. It was found that the pressure changed by 1 bar or less during a typical mixture experiment. This pressure drift correlates to the level of the liquid-helium coolant in the cryostat, and the average pressure and the pressure variations for each measurement could be reconstructed from the recorded helium level.

Due to heat-flush effects and to preferential evaporation of ^{3}He, the concentration changed from its nominal value, and a different pressure was required to match the density to that of pure ^{4}He. The actual ^{3}He concentration was determined from the ratio of the ph-r peak intensities for pure ^{4}He and for the mixtures. At SVP and $T=0.07$ K, we obtained a concentration of $4.7\pm0.2\%$ compared to the nominal (prepared) concentration of 6%. At higher pressures the concentration was lowered as pure ^{4}He was added to pressurize the sample. The ^{3}He concentration also varies slightly with temperature, since the heat-flush effect is temperature dependent. The precision in the concentration determination is limited by systematic effects rather than by the counting statistics of the ph-r peak. The basic assumption is that the ph-r scattering is not modified by the presence of ^{3}He, i.e., ^{3}He is assumed to act only as an absorbing medium (a low-concentration approximation). In fact, the intensity ratio between pure ^{4}He and mixtures varies slightly with the wave vector. This could be due to a contribution from the cross term S_{34} to the scattering. However, even for the 5% mixture this variation is small and corresponds to a concentration error of less than 0.2%, and it is negligible for 1% mixtures. Another limitation is that the nominal sample depth (2.2 mm) is known only to within 5%. The concentrations obtained agree well with the estimated ^{3}He depletion due to heat-flush effects and to preferential evaporation, calculated from the known volumes and temperatures. With the average pressure and concentration determined for each measurement, reliable corrections to the ph-r shift were obtained. These are discussed in detail in Sec. IV.

III. PARTICLE-HOLE EXCITATIONS

The particle-hole (p-h) excitation of ^{3}He in dilute mixtures is seen as a peak at low energies in the scattering function (Figs. 2 and 3). At low concentrations the ^{3}He subsystem can be considered as a nearly noninteracting Fermi gas. The interaction of ^{3}He with the superfluid ^{4}He introduces an effective mass m^*, which reflects the backflow of ^{4}He atoms around a moving ^{3}He atom. Thermodynamic and transport measurements determine the heat-capacity effective mass $m_C^*(p,x_3)$ or the inertial mass $m_I^*(p,x_3,T)$. In the limit $T\rightarrow 0$ and $x_3\rightarrow 0$ both should be equal to the zero-concentration effective mass $m_0^*(p)$. From current theoretical models, $m_0^*(p)$ obtained from heat-capacity measurements differs systematically from that of second-sound (or normal fluid density) measurements. We refer to Polturak and Rosenbaum[25] for a thorough discussion. An approximate value for m_0^*/m_3 in the mixture, in agreement with most measurements, is 2.3 ± 0.2 at SVP, whereas the effective mass is $2.8m_3$ in pure ^{3}He at SVP[26].

A. Line shape

Landau and Pomeranchuk[27] (LP) proposed a quadratic quasiparticle spectrum for a weakly interacting Fermi fluid,

$$E(k)=E_0+\hbar^2k^2/2m^* \ . \tag{10}$$

The scattering function for this excitation is obtained from the Lindhard function.[28] At finite temperature, it is given explicitly by Khanna and Glyde.[29] We have replaced the low-temperature expansion of the chemical potential $\mu(T)$ by the exact $\mu(T)$, obtained by numerically solving the Fermi integral. Data taken at 12.7 bars and $x_3=4.5\%$ at six different temperatures (cf. Table I), were analyzed with this finite-temperature Lindhard function. The scattering function at $Q=1.3$ Å^{-1}, normalized with respect to the ^{3}He scattering cross section, is shown in Fig. 4(a). At this wave vector, $\hat{S}_3(Q,\omega)$ is well separated from both the elastic peak and the ph-r excitation. The negative values of $\hat{S}_3(Q,\omega)$ at energies smaller than 2 K are an artifact of the empty-container correction. The temperature-dependent Lindhard function was folded with the instrumental resolution and fitted to the low temperature ($T=0.07$ K) $\hat{S}_3(Q,\omega)$ with the effective mass, m^*, and the area of the p-h peak, f, as free parameters. The result shown as the solid curve in Fig. 4(a) corresponds to $m^*=2.95m_3$ and $f=0.37$. With no additional parameters, the Lindhard function at higher temperatures was calculated for the same m^* and f [Figs. 4(b)–4(f)]. The agreement with experiment is excellent, especially in view of the large temperature range which is covered ($0.2<T/T_F<4.6$, $T_F=0.32$ K). However, there is an indication that the nearly-free-Fermi-gas model slightly overestimates the broadening with increasing temperature.

The temperature dependence of the 1% mixture was not studied. Data were taken only at 70 mK, which is rather close to the Fermi temperature of about 120 mK at this concentration.

The observed area of the p-h peak at $Q=1.3$ Å^{-1} is only $\frac{1}{3}$ of that expected for a free-Fermi gas. This discrepancy can qualitatively be understood from sum-rule arguments. $S^0(Q,\omega)$ for a free-Fermi gas, obtained from the Lindhard function, fulfills the f-sum rule [Eq. (8)] and has a static-structure factor (zeroth moment)

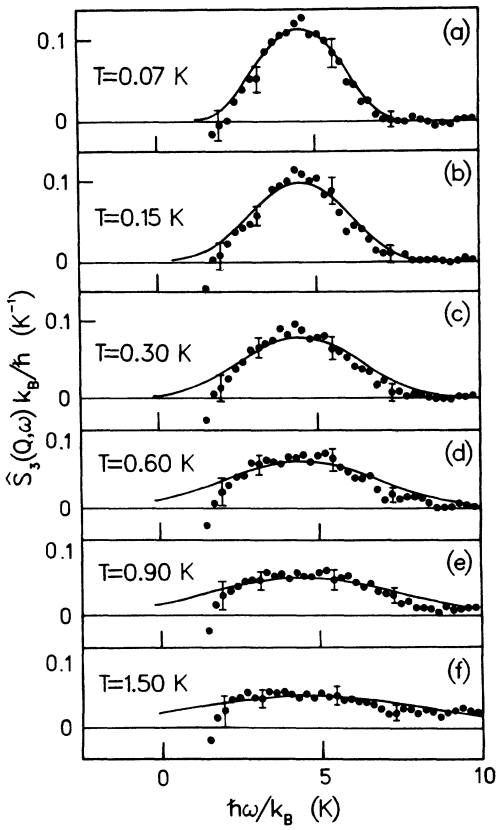

FIG. 4. Temperature dependence of the particle-hole peak. (a) A finite-temperature Lindhard function with the effective mass and the area of the peak as free parameters is fitted to the 5% data at 12.7 bars and $T=0.07$ K. (b)–(f) The solid curves are calculated with the parameters obtained from the fit shown in (a).

$$S(Q)=\int S^0(Q,\omega)d\omega\ , \tag{11}$$

which is 1 for $Q>2k_F$. By using an effective mass m^* in the Lindhard function, the zeroth moment remains unchanged, but the first moment becomes smaller by a factor m/m^*, and hence does not fulfill the f-sum rule. Therefore, additional scattering from the ^{3}He nuclei must take place at higher energies. We suggest that the ^{3}He scattering function can be written as a sum of the p-h scattering function S^* and an additional scattering function S_m,

$$S_3(Q,\omega)=fS^*(Q,\omega)+S_m(Q,\omega)\ , \tag{12}$$

where, for simplicity, we assume

$$S_m(Q,\omega)=Z_m\delta(\omega-\omega_m(Q))\ . \tag{13}$$

Thus, the zeroth moment becomes

$$S_3(Q)=f+Z_m \tag{14}$$

and the f-sum rule yields

$$\frac{\hbar^2Q^2}{2m}=f\frac{\hbar^2Q^2}{2m^*}+Z_m\hbar\omega_m\ . \tag{15}$$

On the assumption that $S_3(Q)=1$, Eqs. (14) and (15) with $f=0.37$ and $m^*=2.95m_3$ yield

$$\hbar\omega_m=1.4\hbar^2Q^2/2m_3=4.1\hbar^2Q^2/2m^*\ .$$

Such a high-frequency resonance in the density-fluctuation spectrum has in fact been predicted by Götze *et al.*[30]

B. Q dependence

For a Fermi gas with a quadratic quasiparticle (qp) energy $E(k)$, the scattering function $S(Q,\omega)$ obtained from the Lindhard function is symmetric for $Q>2k_F$. This implies that the position of the p-h peak $\hbar\omega_{\text{p-h}}(Q)$ coincides with $E(k)$. For a nonquadratic qp energy, $S(Q,\omega)$ becomes asymmetric and the peak position $\hbar\omega_{\text{p-h}}(Q)$ does not coincide with $E(k)$.

To determine $\omega_{\text{p-h}}(Q)$, we have fitted a Gaussian to the low-energy peak of the scattering function at constant wave vector. This is justified since the asymmetry of $\hat{S}_3(Q,\omega)$ is not too large. The position of the Gaussian, which represents $\omega_{\text{p-h}}(Q)$, is plotted in Fig. 5 for the 1% mixture, together with the measured ph-r dispersion. From this and the 5% data we infer a distinct pressure dependence and a rather weak concentration dependence of $\omega_{\text{p-h}}(Q)$. No temperature dependence can be resolved within the precision of the fits. For $Q<0.9$ Å^{-1} the results are influenced by the empty-container correction. For $Q>1.7$ Å^{-1} we do not obtain reliable results, because the p-h peak is smaller and overlaps with the tail of the ph-r peak.

Many attempts to parametrize the qp energy are found in the literature.[25,30–33] They are usually of the form

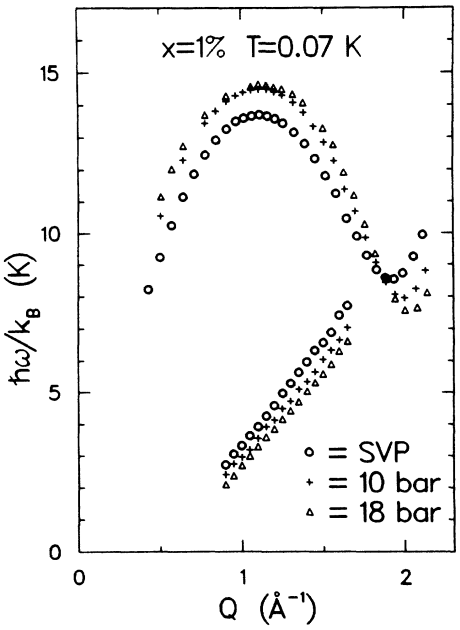

FIG. 5. Excitation spectra for the particle-hole band (lower part) and the phonon-roton branch.

TABLE II. Parameters from the fitting of Eqs. (17) and (18) to the ^{3}He quasiparticle spectrum for concentrations and pressures as given, at $T=0.07$ K. The fitting errors are ± 0.02 in m^*/m_3 and ± 0.01 in the parameters a and b.

x_3 (%)	p (bar)	m^*/m_3	a (Å^2)	m^*/m_3	b (Å^2)
1.0	0.1	2.23	−0.080	2.16	0.114
0.9	10.3	2.50	−0.074	2.45	0.101
0.8	18.2	2.74	−0.065	2.69	0.085
4.7	1.6	2.27	−0.088	2.18	0.132
4.5	12.7	2.51	−0.087	2.43	0.128
4.1	19.5	2.71	−0.076	2.64	0.107

$$E(k)=E_0+\frac{\hbar^2k^2}{2m^*}g(k)\ , \tag{16}$$

where $g(k)$ is a rational function of k. For our purpose and with the precision of the present data, a two-parameter expression is appropriate. We have fitted the expressions

$$\hbar\omega_{\text{p-h}}(Q)=\frac{\hbar^2Q^2}{2m^*}(1+aQ^2) \tag{17}$$

and

$$\hbar\omega_{\text{p-h}}(Q)=\frac{\hbar^2Q^2}{2m^*}\frac{1}{1+bQ^2} \tag{18}$$

to the p-h peak positions for wave vectors $1.0<Q<1.7$ Å^{-1}, with m^* and $a(b)$ as free parameters. The results which are given in Table II display a strong pressure dependence but no concentration dependence of m^*. The values of m^* are close to the zero-concentration limit compiled by Polturak and Rosenbaum.[25] Since m^* is obtained in the limit $Q\to 0$, whereas the actual data are taken at $Q>0.9$ Å^{-1}, some caution in the interpretion of the present results is suggested. This is immediately clear from Fig. 6: Equations (17) and (18) both fit the data well but give rather different values on m^*, although still consistent with other data.[25]

The observed deviation of $\omega_{\text{p-h}}(Q)$ from a simple quadratic form is consistent with the results obtained by Hilton *et al.*[8] (Fig. 7), and the present results are more accurate. Several thermodynamic measurements[25] also imply a deviation from the LP spectrum [Eq. (10)]. In Fig. 8 we compare our results from the 1% mixture at SVP with the qp spectrum derived by Eselson *et al.*[31] from measurements of the normal-fluid density, by Greywall[32] from specific-heat and second-sound measurements, and by Owers-Bradley *et al.*[33] from specific-heat data. Also shown is the calculation by Bhatt[16] where the deviation from the LP spectrum is due to roton emission by ^{3}He excitations. In Fig. 8 the excitation energy is divided by the LP energy for an effective mass of $2.34m_3$, in order to more clearly display the differences between the models. The present direct measurement of the qp spectrum at finite wave vectors is in excellent agreement with the in-

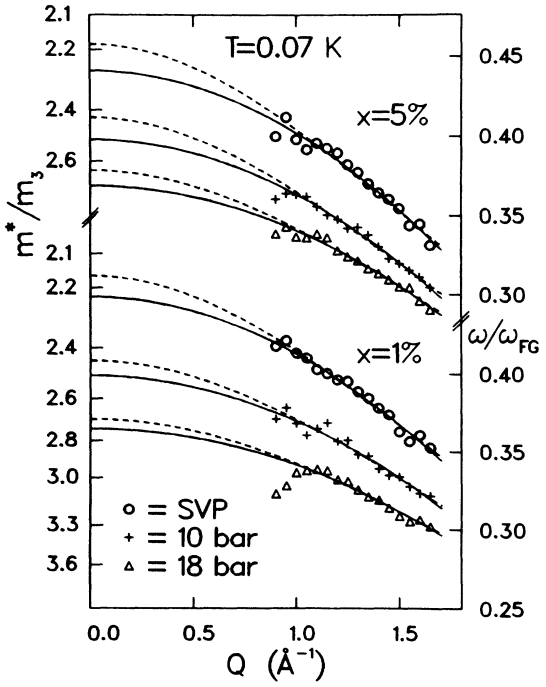

FIG. 6. Energy of the particle-hole excitation divided by the Fermi-gas energy $\hbar\omega_{\text{FG}}=\hbar^2Q^2/2m_3$. Solid (dashed) line is the best fit of Eq. 17 (18).

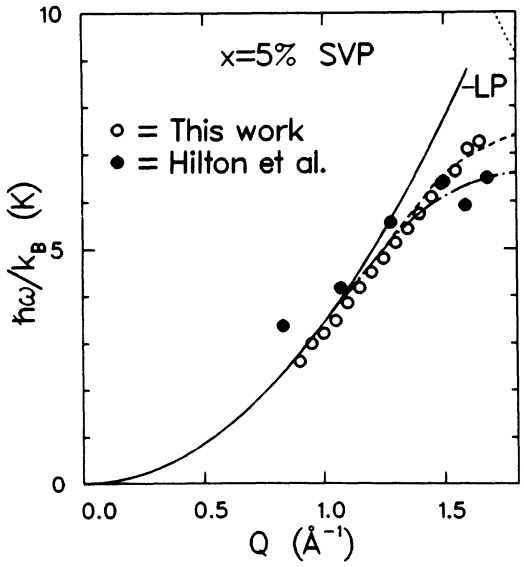

FIG. 7. Energy of the particle-hole excitation. Comparison of the present results ($x_3=4.7\%$, $p=1.6$ bar, $T=0.07$ K) with Hilton *et al.* (Ref. 8; $x_3=6\%$, $p=0$ bar, $T=0.6$ K), and with the LP spectrum using $m^*=2.34m_3$ (solid line). Dashed and dotted-dashed lines are calculations of Hsu *et al.* (Ref. 10) employing the Eselson and Greywall spectra, respectively.

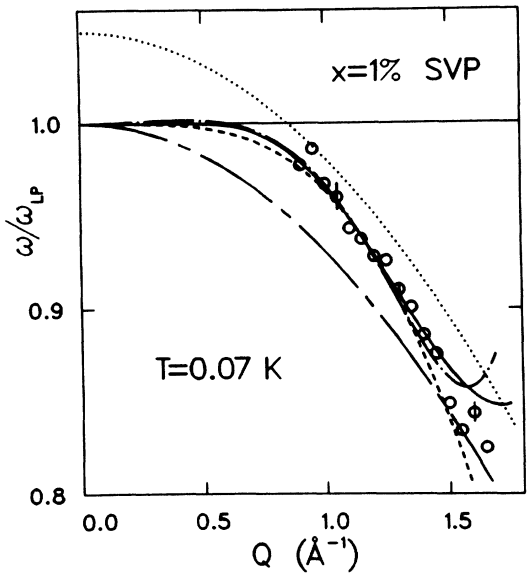

FIG. 8. Energy of the particle-hole excitation divided by $\hbar\omega_{LP}=\hbar^2Q^2/2m^*$ (with $m^*/m_3=2.34$) for $x_3=1\%$. Solid and dashed-dotted lines are the Greywall spectra (fits 1 and 4 in Ref. 32), dashed line is the Eselson spectrum (Ref. 31), dotted line is from Owers-Bradley (Ref. 33), and the long-dashed line is the spectrum calculated by Bhatt (Ref. 16).

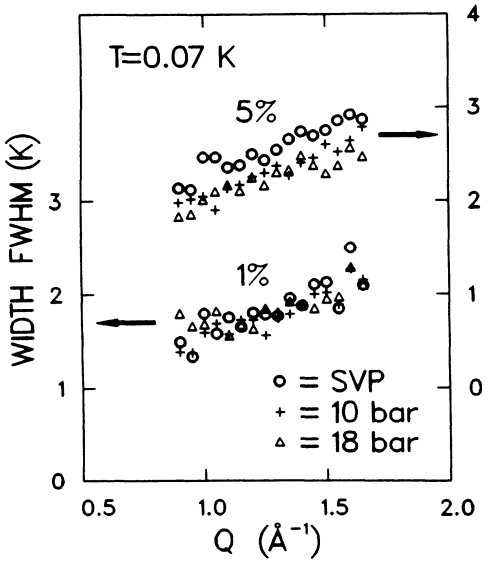

FIG. 9. Intrinsic width of the particle-hole band.

direct determination by Greywall: The two spectra agree to within $\pm1\%$ for wave vectors between 1.0 and 1.45 Å^{-1}. At larger wave vectors the sensitivity of the thermodynamic measurements decreases rapidly. There is no evidence for a rotonlike minimum as suggested by Pitaevskii.[34]

The width of the Lindhard function increases linearly with Q: The full width at half maximum (FWHM) is

$$W=\sqrt{2}\hbar^2k_FQ/m^* . \tag{19}$$

The FWHM of the Gaussian fitted to the data and corrected for instrumental resolution is also approximately linear in Q (Fig. 9), but considerably smaller than predicted by Eq. (19). This remains true even considering the fact that the Gaussian width underestimates the true width of the Lindhard function. The thermal broadening of the p-h band is shown in Fig. 10 for $Q=1.3$ Å^{-1} at 12.7 bars as the FWHM of the observed peak, corrected for instrumental resolution. The solid curve is the width $W\propto Q(T/M)^{1/2}$ for the case of a classical gas (following the Boltzmann distribution) with a particle mass $M=2.74m_3$. Figure 10 illustrates the importance of quantum statistics: The ^{3}He atoms behave like a free gas of fermions in superfluid ^{4}He, and for temperatures well above the Fermi temperature the statistics of this gas is no longer relevant.

The integrated intensity of the p-h excitation, $S_{p\text{-}h}(Q)$, obtained from the Gaussian fit is shown in Fig. 11. In contrast to the free-Fermi-gas model where $S_{p\text{-}h}(Q)$ equals unity for $Q>2k_F$, $S_{p\text{-}h}(Q)$ decreases linearly with Q. This agrees qualitatively with the mode-coupling calculation by Götze *et al.*[30] Within the precision of the measurements, $S_{p\text{-}h}(Q)$ is independent of pressure and concentration.

Hsu *et al.*[10] have calculated the scattering function $S_{p\text{-}h}(Q,\omega)$ for $x_3=6\%$ and $T=0.6$ K. They treat the ^{3}He quasiparticles as a noninteracting gas with a finite lifetime. $S_{p\text{-}h}(Q,\omega)$ is calculated both for the Greywall and for the Eselson qp spectra. The main difference in the results for the two spectra is caused by the difference in the cutoff momentum; namely, the momentum at which it becomes possible for a ^{3}He qp to decay into a roton and a small-Q quasiparticle. Hsu *et al.* find a much larger peak asymmetry with the Eselson spectrum than with the Greywall spectrum. This large asymmetry is not observed in the present results. The Eselson spectrum gives a nearly-Q-independent $S_{p\text{-}h}(Q)$, while the Greywall

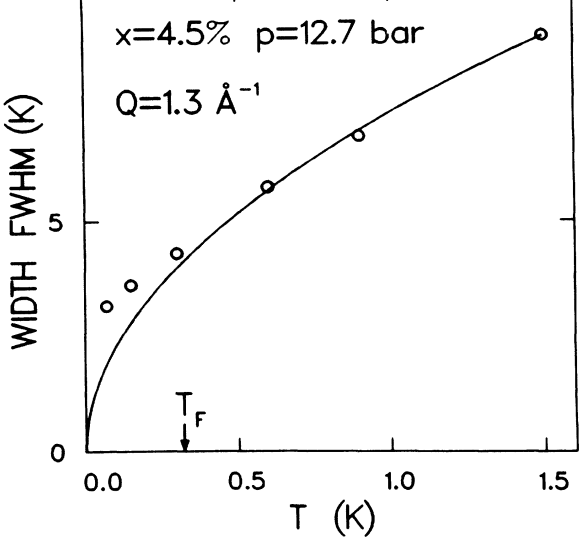

FIG. 10. Temperature dependence of the intrinsic width of the particle-hole band. The solid line is the width of the recoil scattering for a classical gas of atoms of mass $2.74m_3$.

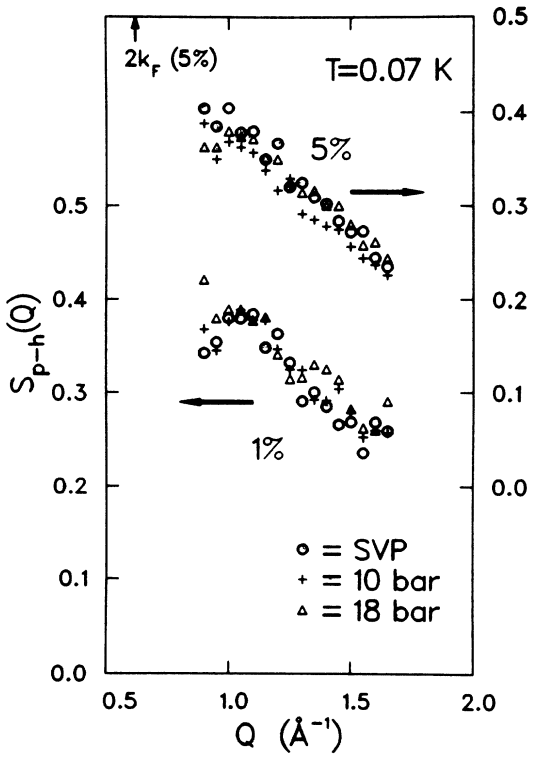

FIG. 11. Static-structure factor for the particle-hole band. For a free Fermi gas $S_{p\text{-}h}(Q)=1$ for $Q>2k_F$.

spectrum predicts a decrease with Q in qualiative agreement with our results. On the other hand, the experimental peak positions are in better agreement with the peak positions calculated from the Eselson spectrum.

C. Crossover

We have seen that with increasing wave vector, the width of the p-h peak increases, the intensity decreases, and the energy approaches the ph-r energy. As illustrated in Fig. 2, the p-h band overlaps with the tail of the ph-r peak for wave vectors larger than 1.6 Å $^{-1}$, and the two components cannot easily be separated. There is no indication that the p-h excitation vanishes at larger wave vectors, however. In fact, a three-dimensional plot of the scattering function where $\hat{S}(Q,\omega)$ is plotted upside down [Fig. 12(a)], reveals that the p-h band continues without appreciable loss of intensity until it enters the ph-r branch, at a wave vector slightly smaller than the roton minimum. An additional indication is given by comparing Figs. 12(a) and 12(b): There is more scattering from the mixture just above the roton minimum. This may indicate that the p-h band continues after crossing the ph-r mode. However, this additional scattering could also be due either to the cross term S_{34} or to increased multiphonon scattering. The multiphonon scattering, which is of similar magnitude as the p-h scattering, is believed to increase due to the additional anharmonicity caused by ^{3}He impurities. It would be of interest to know whether the two excitations eventually separate at wave vectors larger than those covered in the present experiment.

IV. COLLECTIVE EXCITATIONS

A. Fitting procedure

The measured width of the phonon-roton (ph-r) peak incorporates the intrinsic width and the instrumental resolution. The latter arises from a number of contributions: Spread in incoming-neutron energy due to monochromator-crystal mosaic and finite collimation, spread in time-of-flight due to chopper pulse length and to geometrical factors, and finite Q resolution. The total energy resolution changes with Q as shown in Fig. 13. The smooth increase in the width with increasing wave vector is mainly due to sample-size effects. The Q resolution, which is due mostly to finite detector size, induces an additional component to the total resolution of the

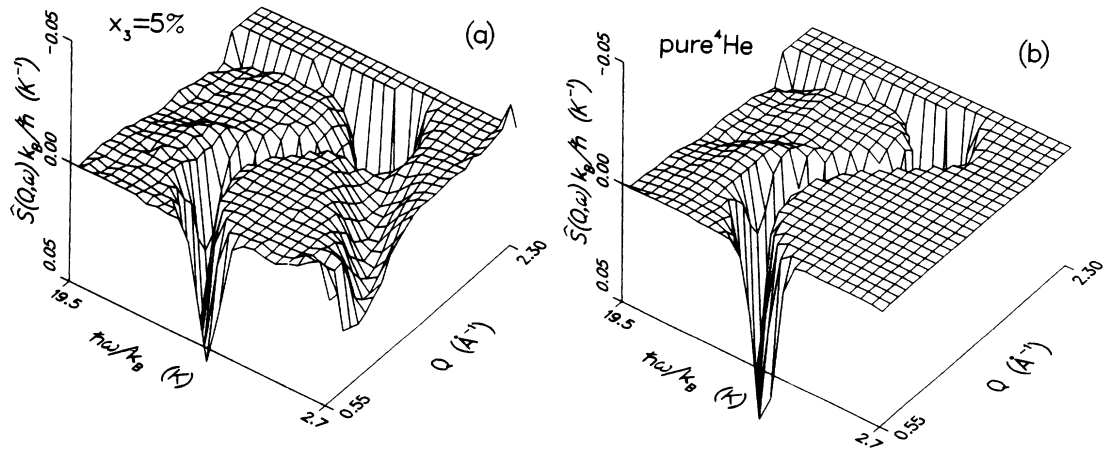

FIG. 12. Neutron-scattering function at SVP and $T=0.07$ K. (a) $x_3=5\%$; (b) pure ^{4}He. $\hat{S}(Q,\omega)$ is plotted upside down to emphasize that the particle-hole band continues until it enters the phonon-roton excitation at a wave vector slightly less than the roton minimum. In (a) the elastic-peak subtraction causes some problems at low energies and the counting statistics is generally worse as indicated by the increased noise in the data. The step at large Q shows the trace of the largest-angle detector in (Q,ω) space.

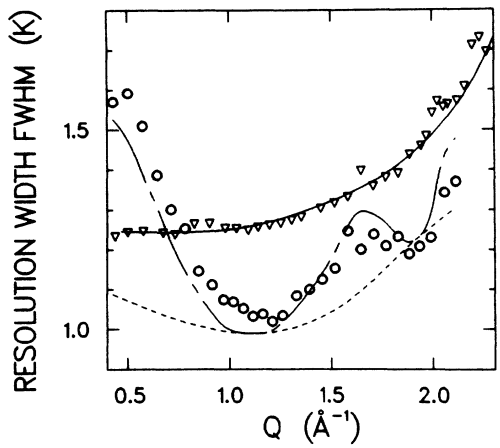

FIG. 13. Resolution at zero-energy transfer: calculated (solid line) and measured with vanadium (triangles). Resolution along the ^{4}He phonon-roton dispersion: measured (circles); calculated, energy resolution only (dashed line) and energy and momentum resolution (long-dashed line). The calculation is from Ref. 21.

ph-r excitation; this component depends on the dispersion and is zero when the dispersion curve has zero slope.

The line shape of the ph-r excitation in pure ^{4}He is taken to be Lorentzian, as was originally proposed by Cohen.[35] At finite temperatures, the scattering function can be written as two Lorentzians multiplied by the temperature factor,

$$S(Q,\omega)=\frac{1}{\pi}\frac{Z_Q}{1-\exp(-\hbar\omega\beta)}\left[\frac{\Gamma_Q}{(\omega-\omega_Q)^2+\Gamma_Q^2}-\frac{\Gamma_Q}{(\omega+\omega_Q)^2+\Gamma_Q^2}\right], \tag{20}$$

which can be rewritten as[36]

$$S(Q,\omega)=\frac{1}{\pi}\frac{Z_Q}{1-\exp(-\hbar\omega\beta)}\times\left[\frac{4\omega\omega_Q\Gamma_Q}{[\omega^2-(\omega_Q^2+\Gamma_Q^2)]^2+4\omega^2\Gamma_Q^2}\right]. \tag{21}$$

This is often referred to as the damped harmonic oscillator (DHO). Tarvin and Passell[37] used a similar form of the DHO suggested by Halley and Hastings,[38] in which $(\omega_Q^2+\Gamma_Q^2)^{1/2}$ was taken to be the ph-r energy. Following Talbot *et al.*,[36] we identify ω_Q with the ph-r energy. However, for $\Gamma_Q \ll \omega_Q$, as in the present case, the difference is small. We also note that the Lorentzians used in Refs. 37 and 39 are not the same as Eq. (20).

In pure ^{4}He the intrinsic width Γ (HWHM) of the roton is very small at low temperatures. In the Landau-Khalatnikov[40] theory the temperature dependence of the width is given by

$$\Gamma=C\sqrt{T}\exp(-\Delta(T)/k_BT), \tag{22}$$

where Δ is the energy of the roton minimum and C is a constant. Equation (22) is in agreement with the neutron spin-echo measurements by Mezei.[41] At the lowest temperature in these measurements, $T=0.96$ K, the width is less than 0.01 K. Thus, the width at $T=0.07$ K is completely negligible compared to the instrumental resolution (HWHM) of approximately 0.5 K in the present experiment. The width of the ph-r peak in pure ^{4}He at temperatures below 0.9 K, obtained by fitting a Gaussian to the data, thus represents the instrumental resolution at a particular energy and wave vector. We refer to such a low-temperature pure-^{4}He measurement as a "reference run."

The energy and width of the ph-r excitation in mixtures, and in ^{4}He at higher temperatures, was obtained by fitting a DHO [Eq. (21)] folded with the Gaussian resolution to the scattering function at constant angle. The height, width, and position of the DHO were used as free parameters. We find that the DHO provides an excellent fit to the observed intensity in the one-phonon region of both pure ^{4}He and mixtures. A typical fit is shown in Fig. 14(a). The intrinsic width (HWHM) of the ph-r excitation is identified with Γ_Q of Eq. (21). The width is identical to the broadening of the ph-r peak since pure ^{4}He has negligible linewidth. The energy shift $\delta\omega_Q$ of the

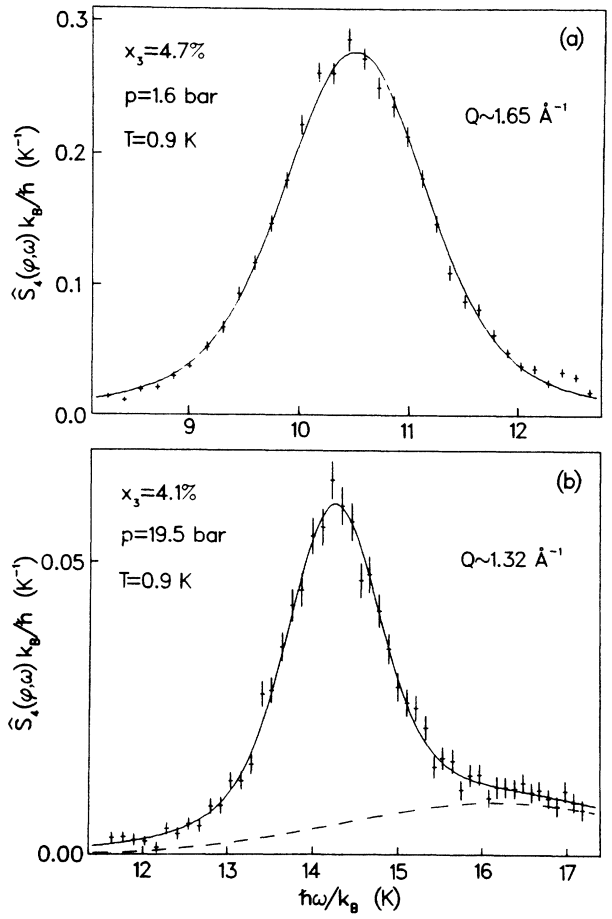

FIG. 14. Typical fits of the damped harmonic oscillator folded with the resolution Gaussian to $\hat{S}_4(\phi,\omega)$. (a) $p=1.6$ bar and $Q=1.65$ Å^{-1}. (b) $p=19.5$ bar and $Q=1.32$ Å^{-1}. The dashed line in (b) is the multiphonon Gaussian.

ph-r excitation is defined as the difference between ω_Q of the DHO and the position of the Gaussian fitted to the reference run, cf. Eq. (2).

Woods and Svensson[42] have suggested an alternative method to analyze the ph-r excitation, in which the scattering function is decomposed into a superfluid component and a normal-fluid component. This *ad hoc* approach, based on assumptions with little theoretical foundation,[43] describes SVP data well. However, recent measurements at 20 bars (Refs. 36 and 44) are not as well described by this model. For a recent thorough discussion of this approach, see Talbot *et al.*[36]

In some cases, especially for Q values in the "maxon" region at high pressures, the multiphonon contribution is large and adds appreciable intensity to the high-energy tail of the one-phonon peak. The low-energy part of the multiphonons will therefore appear to offset and broaden the ph-r peak. At pressures up to 10 bars this effect is negligible compared to the statistical errors in the data. At 18 bars, the multiphonon scattering is stronger and merges with the one-phonon peak. It is therefore necessary to account for the multiphonon contribution in this case. We assume that the intensity of the multiphonon spectrum is zero for energies lower than those of the one-phonon peak,[24,45] and gradually increases with energy until it reaches a maximum, which may be due either to a two-roton or to a maxon-roton excitation. This part of the multiphonon spectrum is described by a rather wide Gaussian of FWHM of typically 4 K. Two Gaussians are therefore fitted to the low-temperature pure-^{4}He spectrum at 18 bars [Fig. 14(b)]: the resolution function and the multiphonon Gaussian with height, width, and position as free parameters. We further assume that the shape of the multiphonon spectrum does not change substantially with temperature or by the presence of ^{3}He impurities. Thus, the width and position of the multiphonon Gaussian were kept fixed in the fits to the high-temperature ^{4}He data and the mixture data. Only the height was left as a free parameter to account for the increased weight of the multiphonon spectra as well as for possible errors in the absolute normalization between different experimental runs (mainly arising from the absorption correction which is sensitive to the absolute concentration).

B. Corrections

The shifts and widths of the ph-r excitation obtained as described above are, in general, very small. Corrections are made for three subtle experimental effects: sample geometry, constant number density, and transformation to constant Q. These corrections are now described.

The "effective" geometry of the pure-^{4}He samples differs from that of the mixtures because of the large-absorption cross section of ^{3}He. The ^{4}He scatters nearly uniformly throughout the bulk of the sample, while mixtures rich in ^{3}He scatter predominantly near the surface. This slightly shifts the average scattering center leading to a difference in time of flight and, hence, an artificial shift in the observed energy transfer. In order to include the transmission of the IN6 radial collimator, which also affects the scattering center, a Monte Carlo simulation

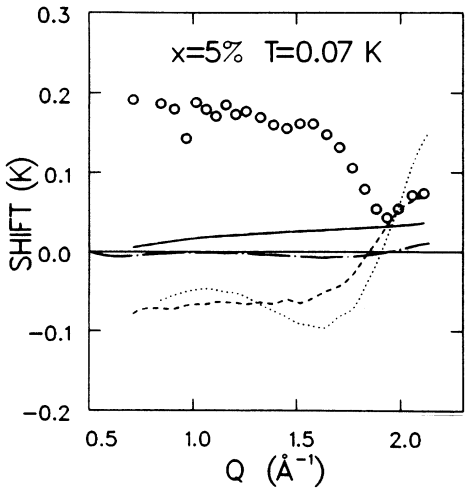

FIG. 15. Corrections to the shift of the phonon-roton excitation. Geometry correction (solid line). Density correction: SVP (dashed line); 10 bars (dotted line); 18 bars (dashed-dotted line). Circles are the fully corrected shifts at SVP.

was used to calculate the geometrical correction to the shift. This correction, shown in Fig. 15 as a solid line, is rather small and increases monotonically with Q. The fact that the neutron-path length is longer in pure ^{4}He than in mixtures leads to an apparent broadening of the ^{4}He–ph-r peak. The width of the resolution Gaussian from the reference run was corrected for this geometry effect before it was folded with the DHO and fitted to the mixture data as described earlier.

Due to pressure drifts and concentration changes during the experiment (cf. Sec. II), the number density of the mixture is slightly different from that of ^{4}He. We have therefore interpolated the pure-^{4}He–ph-r energy to the number density of the mixture in order to determine the ph-r shift at constant density. The interpolation is based on the empirical expression

$$\omega_Q(p)-\omega_Q(0)=A_Q y^2+B_Q y \ , \tag{23}$$

which was fitted to the measured ^{4}He ph-r energies at four different pressures (0, 5, 10, and 18 bars). Here A_Q and B_Q are fitting parameters and

$$y=N_A^{1/3}(V_4(p)^{-1/3}-V_4(0)^{-1/3}) \ , \tag{24}$$

where $1/y$ is the change of the average interatomic distance with pressure, $V_4(p)$ is the ^{4}He molar volume taken from Greywall,[46] and N_A is Avogadro's number. The rms error in the fit was less than 0.01 K. The sign of this correction depends on the wave vector and also on the particular experimental run; examples are shown in Fig. 15, together with the fully corrected shift at SVP. We have not applied this correction to the data taken at 1.5 K.

The pressure fluctuations which occurred during an individual run, and which are caused by variations in the level of the liquid helium coolant, give rise to a broadening of the ph-r peak. However, this additional broadening is comparable to or smaller than the statistical errors in the determination of the widths and, hence, negligible.

Finally, the widths which are obtained from fits to constant-angle scans are also converted to widths at constant Q, by application of the appropriate Jacobian.[47]

The corrections to the ph-r shift and broadening described above are estimated to be reliable at the level of 0.02 K.

C. Results

We now summarize the results for the ph-r excitation in pure ^{4}He and in mixtures. The ^{4}He dispersion at SVP and $T=0.07$ K agrees within 1.5% with the compilation of Donnelly *et al.*[48] The pressure dependence of the roton minimum and the maxon agrees well with the results of Dietrich *et al.*,[39] Graf *et al.*,[45] and Stirling.[49] At $T=1.5$ K there is a definite shift and a broadening of the ph-r peak in agreement with the high-precision neutron spin-echo measurements by Mezei,[41] while at $T=0.9$ K no changes from the low-temperature data are observed. These observations are in semiquantitative agreement with the Landau-Khalatnikov theory,[40] cf. Eq. (22).

The shift $\delta\omega_Q$ of the ph-r peak in mixtures containing 5% ^{3}He is shown in Fig. 16. At low temperatures the shift is always positive and in the range 0.1–0.2 K, and nearly constant for wave vectors smaller than 1.5 Å^{-1}. At SVP $\delta\omega_Q$ begins to decrase at $Q=1.6$ Å^{-1} (1.7 Å^{-1} at 10 and 18 bars) and reaches a minimum near the roton minimum (at respective pressure), before it increases again. At higher temperatures, $\delta\omega_Q$ is smaller by a constant amount such that the pronounced structure remains. The shift at the roton minimum becomes negative already for a small increase in temperature.

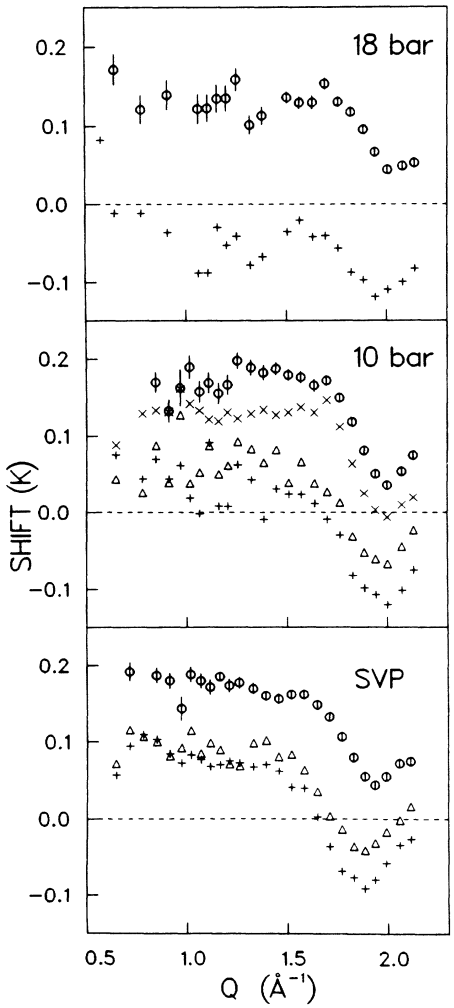

FIG. 16. Phonon-roton shift at constant density at $x_3=5\%$ and different pressures and temperatures. $T=0.07$ K (○), 0.30 K (×), 0.60 K (△), and 0.90 K (+). The statistical errors are shown for the low-temperature data only.

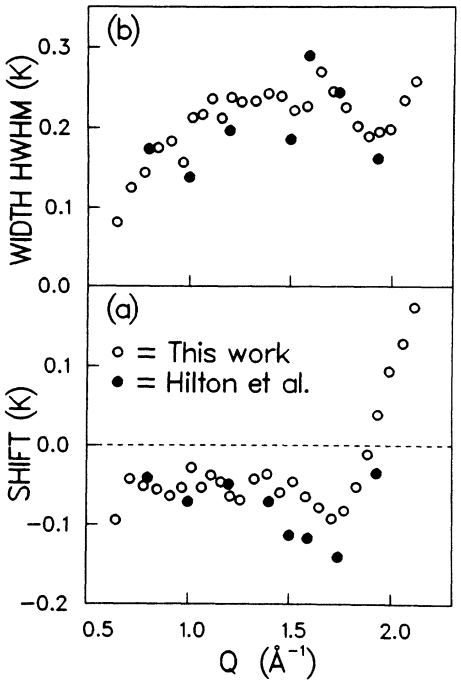

FIG. 17. (a) Shift at constant pressure and (b) linewidth of the phonon-roton excitation at $T=0.6$ K. The present results ($x_3=4.7\%$ and $p=1.7$ bar) are compared with Hilton *et al.* (Ref. 8; $x_3=6\%$ and $p=0$ bar).

The ph-r shifts reported by Rowe *et al.*[7] and by Hilton *et al.*[8] are determined at constant pressure and cannot be compared directly with the present results at constant density. However, through Eqs. (23) and (24) we can interpolate the ^{4}He–ph-r energies to the *same* pressure as the mixture and recalculate the shifts [Fig. 17(a)]. Our results then confirm the results of Hilton *et al.* while they disagree with the results of Rowe *et al.* We note in passing that if the geometry correction described above is applied to the data of Hilton *et al.* (they used a sample container of similar dimensions), the agreement is even better.

For the 1% mixture, no shifts are observed at 10 and 18 bars within the precision of the data, while at SVP there is a shift for $Q>1.8$ Å^{-1} of less than 0.05 K. However, this shift is too small for a quantitative analysis.

The ph-r excitation is clearly broadened in the 5% mixture compared to pure ^{4}He. This was also observed by Hilton *et al.*[8] for temperatures between 0.6 and 1.55 K, and our results are in good agreement with theirs [Fig. 17(b)]. At temperatures below the Fermi temperature, the intrinsic linewidth Γ_Q shows a well-defined maximum

at a wave vector somewhat smaller than the roton minimum. At slightly larger wave vectors there is a minimum in Γ_Q, which was also observed by Rowe *et al.*[7] The maximum and the minimum both move to larger wave vectors as the pressure is increased, similar to the roton minimum (Fig. 18). With increasing temperature, Γ_Q increases, the minimum moves to smaller wave vectors, and the maximum gradually disappears. The linewidth of the maxon increases more rapidly with temperature than the roton linewidth. We find that the width is proportional to T for wave vectors less than $Q=1.7$ Å^{-1}, while it is porportional to $T^{1/2}$ for $Q>1.85$ Å^{-1}.

The ph-r broadening is very small in the 1% mixture and could not be obtained from the fitting procedure used for the 5% mixture. Instead, the width of the ph-r peak from a Gaussian fit was used as the width of a Voigt function, the convolution of a Gaussian and a Lorentzian. The Lorentzian width (HWHM) was then determined using the Gaussian width from the reference run (corrected for geometry broadening). The linewidth obtained in this way shows a distinct structure, similar to that in the 5% data (Fig. 19).

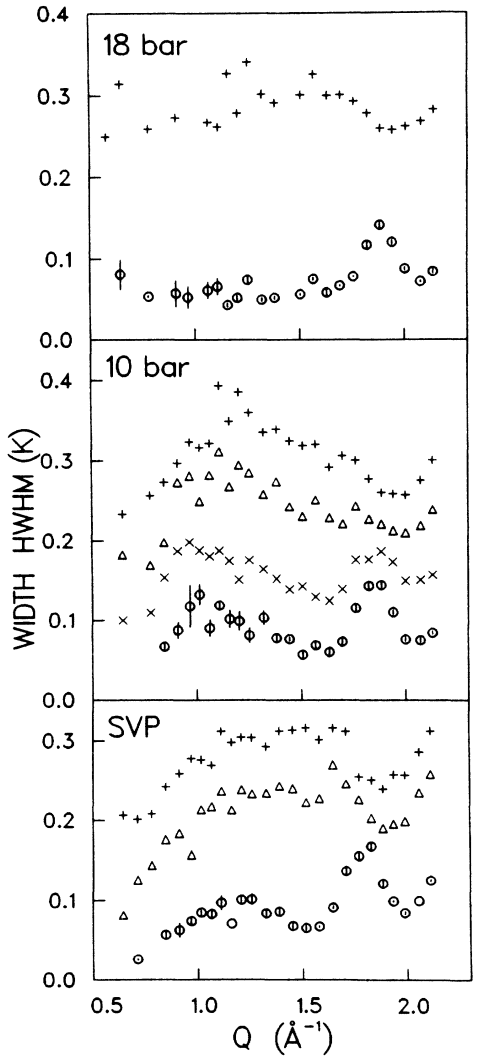

FIG. 18. Phonon-roton linewidth for $x_3=5\%$ and for different pressures and temperatures. Symbols are as in Fig. 16.

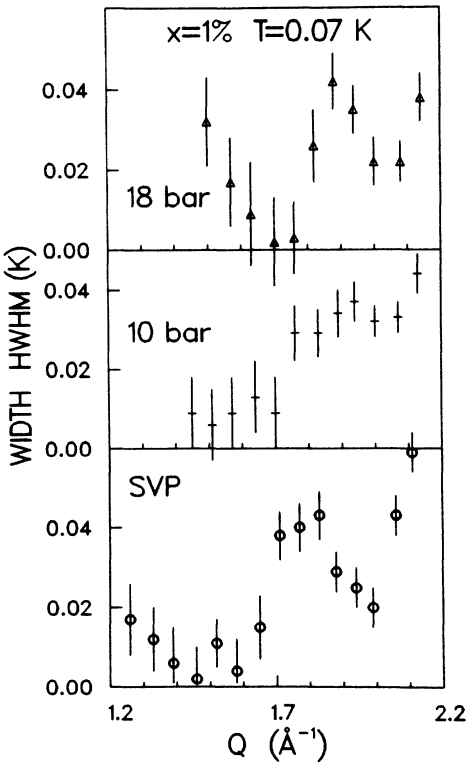

FIG. 19. Phonon-roton linewidth for $x_3=1\%$.

V. DISCUSSION

A. Shift and broadening

The ^{4}He phonon-roton excitation spectrum is modified by the presence of ^{3}He impurities in dilute mixtures. There are four different mechanisms which lead to a shift in the energy and an increase in the linewidth.

(i) The ph-r excitation can be annihilated by creating a particle-hole pair. This three-particle process (3PP), which is analogous to Landau damping in pure ^{3}He, may be interpreted as mode repulsion due to hybridization of the ph-r excitation with the p-h band. It yields a shift and a broadening of the ph-r peak, which can be written as[10]

$$\delta\omega_Q = nZ_Q u_Q^2 \mathrm{Re}[\chi_{33}(Q,\omega_Q)] \tag{25a}$$

and

$$\Gamma_Q = nZ_Q u_Q^2 \mathrm{Im}[\chi_{33}(Q,\omega_Q)] , \tag{25b}$$

where n is the number density, Z_Q is the one-phonon static structure factor, and u_Q is the effective ^{3}He–(ph-r) interaction. χ_{33} is the generalized p-h susceptibility, which is evaluated at the ph-r energy ω_Q. It is related to the scattering function through $S(Q,\omega)=\mathrm{Im}[\chi(Q,\omega)]/\pi$. On the assumption that u_Q is real, the ph-r excitation will be damped only within the p-h band.

(ii) ph-r excitations can also scatter from ^{3}He atoms,

leaving an excited p-h pair and a ph-r excitation after the scattering. This four-particle process (4PP) contributes to the damping at all wave vectors and leads to a shift which probably is comparable in magnitude to the shift due to mechanism (i).

(iii) The cross term S_{34} is expected to contribute predominantly within the ph-r peak. The resulting distortion of the line shape[9] would then lead to a change in the position and in the width of the peak.

(iv) The larger zero-point motion of the ^{3}He atoms reduces the density of the mixture. This reduces the interatomic forces which in turn affects the ph-r energy and scales the wave vector according to Eq. (1). In the present experiment where the mixture and the pure ^{4}He were measured at the same density, this effect will not contribute to the shift.

In the following we compare our experimental results with several published calculations based on the mechanisms (i)–(iv). We also present a calculation of the shift and broadening due to phonon annihilation (i).

B. Comparison with theoretical calculations

Bartley *et al.*[11,12] calculated the ph-r shift due to phonon annihilation [mechanism (i) above]. In their first paper,[11] they assumed that the qp spectrum intersected the ph-r curve. The interaction was obtained from quantum hydrodynamics (QHD) and was characterized by a single coupling constant γ with no wave-vector dependence. They found that the roton spectrum splits into two distinct branches, separated by 10 K at the roton minimum for $x_3=1\%$. This is clearly not in accordance with the experimental results. In a second paper[12] they introduced a wave-vector-dependent interaction, which reduces to the QHD in the limit $Q\rightarrow 0$. The ph-r shift was calculated as a function of both concentration and temperature for two cases: intersecting and nonintersecting spectra. For nonintersecting spectra, they found a positive shift which decreases with increasing temperature. This temperature dependence agrees qualitatively with the present results, but we have found strong evidence that the spectra actually are intersecting. For the case of intersecting spectra, they found that the shift oscillates with Q, in agreement with our results. However, the temperature dependence obtained by Bartley *et al.* is not consistent with the present observations.

Bagchi and Ruvalds[13] calculated the shift and broadening of the ph-r excitation due to both phonon annihilation (i) and to phonon scattering (ii). The corresponding phenomenological coupling constants Γ_3 and Γ_4 were estimated from experiment. In contrast to earlier work, the phonon-scattering contribution was calculated to all orders in the interaction. Ruvalds *et al.*[14] later improved the phonon-annihilation contribution by replacing $|\Gamma_3|^2$ by $nS_Q u_Q^2$ [cf. Eq. (25)], where S_Q is the ^{4}He total-static-structure factor. For u_Q they used the Fourier transform of a square-well potential. Their results are in qualitative agreement with the present experiment.

Donnelly *et al.*[15] calculated the roton shift as a function of temperature and concentration using a dielectric model for the roton interaction. Since their calculation assumes constant number density, it should be directly comparable to the present results. However, it reproduces neither the sign nor the pronounced wave-vector dependence of the shift.

Lücke and Szprynger[9] calculated the roton shift due to phonon annihilation, the cross term S_{34}, and the reduced density [i.e., mechanisms (i), (iii), and (iv)]. Their calculation is in good agreement with the results of Hilton *et al.*[8] for wave vectors larger than 1.5 Å^{-1}. Before comparing to the present results, the largest contribution to the shift in the calculation in Ref. 9, the reduced density, has to be removed. We have not been able to do so from the information given in the paper.

The temperature- and concentration-dependent ph-r shift has been calculated by Hsu *et al.*[10] They used the Aldrich-Pines pseudopotentials (cf. Ref. 10) to evaluate the shift due to phonon annihilation (i) and reduced density (iv). The phonon-scattering process (ii) was included in a rather approximate way. The results are in remarkably good agreement with those of Hilton *et al.*[8] In Fig. 20 we compare our results with the calculated shift due to phonon annihilation and scattering only. The pronounced Q dependence of the shift is rather well reproduced as far as the shape is concerned, but the curve is shifted in Q. At zero temperature the ph-r linewidth due to phonon annihilation [Eq. (25b)] is 1 order of magnitude smaller than the total linewidth observed in the present experiment. The broadening at higher temperatures due to phonon scattering shows no structure in Q in the theoretical results of Hsu *et al.*

C. Landau damping

We have calculated the shift and the broadening of the ph-r excitation due to Landau damping [i.e., phonon annihilation (i)] from Eq. (25). For a gas of noninteracting fermions, the quasiparticle spectrum is parabolic and χ_{33} is given by the Lindhard function. To account for the deviation from a parabolic spectrum, we have introduced a Q-dependent effective mass $m^*(Q)=m^*/(1+aQ^2)$ [cf.

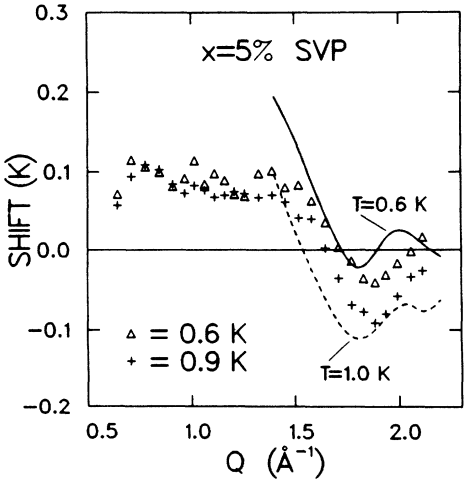

FIG. 20. Phonon-roton shift at constant density (symbols) compared to the calculation by Hsu *et al.* (Ref. 10; solid and dashed lines). See text for details.

Eq. (17) and Table II] in the final (closed) expression for the zero-temperature Lindhard function. This neglects the asymmetry of χ_{33} caused by the nonparabolic spectrum but is a good approximation for the peak position of χ_{33} and also for the narrowing of the p-h band. The results of the calculation are much more sensitive to small changes of the potential parameters than to the details of χ_{33}, as long as the qp spectrum crosses the ph-r curve at a Q value slightly lower than that of the roton minimum. This observation simply reflects the wide Q range of the crossover region between the ph-r mode and the rather broad p-h band. (The width in Q of the p-h band is approximately $2k_F$, which for $x_3=4.7\%$ is 0.62Å^{-1}).

We use the one-phonon structure factor Z_Q from the present ^{4}He measurements and the Fourier transform of a square-well potential of height 35 K for u_Q in the calculation. In Fig. 21 we show the results for two different ranges a of the potential. For wave vectors larger than 1.2 Å^{-1}, the potential with $a=2.46$ Å predicts shifts identical with those of the polarization potential from Ref. 10, except for a scaling factor. (Hsu *et al.* obtain shifts different from this because of a very different choice of χ_{33}.) The structure in $\delta\omega_Q$ agrees very well with the experimental results [Fig. 21(a)]. To reproduce the observed linewidth [Fig. 21(b)] a potential with a shorter range ($a=2.30$ Å) is required. In Fig. 21 a constant of 0.08 K (0.06 K) is added to the shift (linewidth), as indicated by the dotted lines. This is certainly an oversimplification of the contribution from the phonon scattering process (ii), which is not included in the calculation, but which can be expected to give a nearly Q-independent contribution. We believe that the linear increase in linewidth with temperature observed for $Q<1.7$ Å^{-1} is due to this process, as well as the Q-independent offset of the shift at higher temperatures. We find that a potential which describes the broadening does not reproduce the shift, and vice versa. This may indicate that a potential with an imaginary part is needed in this model. We have also calculated the broadening at higher temperatures by using the temperature-dependent Lindhard function[29] in Eq. (25b), but with the same potential. The displacement of the maximum in Γ_Q towards smaller wave vectors (cf. Fig. 18) is qualitatively reproduced while, as can be expected, the overall Q-independent increase in the linewidth is not.

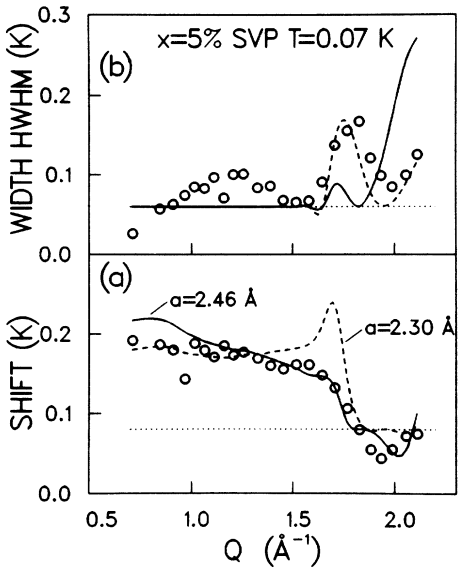

FIG. 21. (a) Shift at constant density and (b) linewidth of the phonon-roton excitation. Circles are experimental data. Solid (dashed) line is from a phonon annihilation calculation with a square-well potential of height 35 K and range $a=2.46$ Å ($a=2.30$ Å). The dotted horizontal line is an offset approximating the contribution from the phonon-scattering process.

Our calculations suggest that the qp spectrum crosses the ph-r branch near the roton minimum and also show that the shift and linewidth are very sensitive to the choice of potential. This implies that the present experimental results can be used to determine the ^{3}He–(ph-r) interaction. A better representation of χ_{33} at finite temperatures for noninteracting fermions with a nonparabolic spectrum would certainly improve the calculation. Finally, we like to point out that even though the phonon-annihilation process describes the structure in $\delta\omega_Q$ and Γ_Q, other mechanisms such as phonon scattering or the cross term S_{34} may provide alternative explanations.

D. The cross term

In this paper we have assumed that the cross term $S_{34}(Q,\omega)$ is so small that the low- and high-energy peaks in $\hat{S}(Q,\omega)$ can be identified with ^{3}He–p-h and ^{4}He–ph-r excitations, respectively. S_{34} was also neglected in our interpretation of the ph-r shift and broadening in terms of phonon-annihilation and scattering processes. This assumption is not obvious. In fact, the prefactor of S_{34} is rather large and the contribution could be substantial. However, there is no direct evidence of the cross term in $\hat{S}(Q,\omega)$. The small amount of extra scattering above the roton minimum [Fig. 12(a)] could arise from S_{34}, but also from p-h or multiphonon scattering. If the shift and broadening were due to S_{34} only, the ph-r peak would show a clear asymmetry because S_{34} changes sign there.[9] This is related to the vanishing first moment of S_{34}, Eq. (8a). However, no such asymmetry of the ph-r peak is observed. Improved calculations of $S_{34}(Q,\omega)$ would assist in clarifying this point.

VI. CONCLUSIONS

We have measured the neutron-scattering function for dilute mixtures of 1% and 5% ^{3}He in superfluid ^{4}He at pressures of 0, 10, and 18 bars. The measurements were performed at several temperatures between 0.07 and 1.5 K, and thus represents the first neutron-scattering measurement on mixtures below the Fermi temperature. The excitation spectrum has two well-defined branches: a collective ^{4}He–phonon-roton mode and a ^{3}He–particle-hole band.

The ^{3}He quasiparticle spectrum, which is measured directly in a neutron-scattering experiment, deviates from a simple quadratic form. This is in very good agreement

with the spectrum derived from thermodynamical measurements by Greywall and by Eselson *et al.* The qp spectrum shows no rotonlike minimum, and there are strong indications of a crossover with the collective ph-*r* excitation. The line shape of the p-h excitation is well described at all temperatures by a nearly-free-Fermi-gas model with a Q-dependent effective mass. A complete description of the line shape of the p-h excitations should include the calculation of the generalized susceptibility for a nonparabolic spectrum. This is beyond the scope of this work, however.

The ph-r excitation in mixtures was analyzed by fitting to the scattering function the convolution of a damped harmonic oscillator (or two Lorentzians) with the resolution function obtained from the results for pure ^{4}He. The extracted shift and broadening of the ph-r excitation were corrected for several systematic effects related to the experimental conditions. The mixtures were measured at a slightly higher pressure than that of pure ^{4}He, such that the number density remained the same for the two systems. In this way one can more easily compare the experimental results with theoretical calculations. At low temperatures we find a pronounced structure in the shift and width of the ph-r excitation at wave vectors near the crossover with the p-h spectrum. At higher temperatures the structure in the shift remains while it gradually disappears in the width. With increasing pressure this structure moves to larger wave vectors as does also the crossover region. These results are compared to several published theoretical results, as well as to our own calculations of the ph-r shift and broadening due to phonon annihilation (Landau damping). Our calculations reproduce the main features of the experimental results, in particular, the Q-dependent structure. However, for agreement with the experimental results the calculations of the shift and the calculations of the linewidth require different potential parameters. At present, there is no theory which satisfactorily describes both the shift and the linewidth of the ph-r mode. It is our hope that this work will stimulate further theoretical calculations of the interactions between elementary excitations in liquid-helium mixtures.

ACKNOWLEDGMENTS

The invaluable technical assistance of Y. Blanc, F. Hennecke, and W. Heinemann is gratefully acknowledged. Special thanks are due to J. L. Ragazzoni and the cryogenic laboratory at the ILL for their assistance and hospitality. We have benefited from useful discussions with R. Ghosh, H. Godfrin, K. Sköld, and W. G. Stirling. This work was supported in part by the Swedish Natural Science Research Council and by the German Federal Ministry for Research and Technology under Contract No. 03-SC1 PTB-6.

---

*Present address: Institut Laue-Langevin, 38042 Grenoble, France.

†Present address: Max-Planck-Institut, Mainz, FRG.

[1]H. R. Glyde and E. C. Svensson, in *Neutron Scattering,* Vol. 23B of *Methods of Experimental Physics,* edited by D. L. Price and K. Sköld (Academic, New York, 1987), p. 303, and references therein.

[2]R. Scherm, K. Guckelsberger, B. Fåk, K. Sköld, A. J. Dianoux, H. Godfrin, and W. G. Stirling, Phys. Rev. Lett. **59**, 217 (1987).

[3]R. Scherm, A. J. Dianoux, B. Fåk. K. Guckelsberger, M. Körfer, and W. G. Stirling, Physica **156-157B**, 311 (1989).

[4]D. W. Hess and D. Pines, J. Low Temp. Phys. **72**, 247 (1988).

[5]A. Holas and K. S. Singwi, Phys. Rev. B **40**, 167 (1989).

[6]F. Dalfovo and S. Stringari, Phys. Rev. Lett. **63**, 532 (1989).

[7]J. M. Rowe, D. L. Price, and G. E. Ostrowski, Phys. Rev. Lett. **31**, 510 (1973).

[8]P. A. Hilton, R. Scherm, and W. G. Stirling, J. Low Temp. Phys. **27**, 851 (1977); R. Scherm, W. G. Stirling, and P. A. Hilton, J. Phys. (Paris) Colloq. **39**, C6-198 (1978).

[9]M. Lücke and A. Szprynger, Phys. Rev. B **26**, 1374 (1982); A. Szprynger and M. Lücke, *ibid.* **32**, 4442 (1985).

[10]W. Hsu, D. Pines, and C. H. Aldrich III, Phys. Rev. B **32**, 7179 (1985).

[11]D. L. Bartley, J. E. Robinson, and V. K. Wong, J. Low Temp. Phys. **12**, 71 (1973).

[12]D. L. Bartley, V. K. Wong, and J. E. Robinson, J. Low Temp. Phys. **17**, 551 (1974).

[13]A. Bagchi and J. Ruvalds, Phys. Rev. A **8**, 1973 (1973).

[14]J. Ruvalds, J. Slinkman, A. K. Rajagopal, and A. Bagchi, Phys. Rev. B **16**, 2047 (1977).

[15]R. J. Donnelly, R. W. Walden, and P. H. Roberts, J. Low Temp. Phys. **31**, 375 (1978).

[16]R. N. Bhatt, Phys. Rev. B **18**, 2108 (1978).

[17]D. L. Price and K. Sköld, in *Neutron Scattering,* Vol. 23A of *Methods of Experimental Physics,* edited by K. Sköld and D. L. Price (Academic, New York, 1986), p. 1.

[18]V. F. Sears, in *Neutron Scattering,* Vol. 23A of *Methods of Experimental Physics* (Ref. 17), p. 521.

[19]K. S. Pedersen and R. A. Cowley, J. Phys. C **16**, 2671 (1983).

[20]Y. Blanc, Institut Laue-Langevin Report No. 83BL21G, 1983.

[21]K. Guckelsberger, Y. Blanc, A. J. Dianoux, B. Fåk, H. Godfrin, M. Körfer, R. Scherm, and K. Sköld, Physica **156-157B**, 681 (1989).

[22]M. Körfer, R. Scherm, K. Guckelsberger, and B. Fåk (unpublished).

[23]V. F. Sears, Nucl. Instrum. Methods **123**, 521 (1975).

[24]E. C. Svensson, P. Martel, V. F. Sears, and A. D. B. Woods, Can. J. Phys. **54**, 2178 (1976).

[25]E. Polturak and R. Rosenbaum, J. Low Temp. Phys. **43**, 477 (1981), and references therein.

[26]D. S. Greywall, Phys. Rev. B **33**, 7520 (1986).

[27]L. D. Landau and I. Pomeranchuk, Dokl. Akad. Nauk SSSR **59**, 669 (1948).

[28]J. Lindard, Dan. Mat. Fys. Medd. **28**, 8 (1954).

[29]F. C. Khanna and H. R. Glyde, Can. J. Phys. **54**, 648 (1976).

[30]W. Götze, M. Lücke, and A. Szprynger, Phys. Rev. B **19**, 206 (1979).
[31]B. N. Eselson, V. A. Slyusarev, V. I. Sobolev, and M. A. Strzhemechnyi, Pis'ma Zh. Eksp. Teor. Fiz. **21**, 253 (1975) [JETP Lett. **21**, 115 (1975)]; Fiz. Nizk. Temp. **2**, 418 (1976) [Sov. J. Low Temp. Phys. **2**, 207 (1976)].
[32]D. S. Greywall, Phys. Rev. Lett. **41**, 177 (1978); Phys. Rev. B **20**, 2643 (1979).
[33]J. R. Owers-Bradley, P. C. Main, R. M. Bowley, G. J. Batey, and R. J. Church, J. Low Temp. Phys. **72**, 201 (1988).
[34]L. P. Pitaevskii (unpublished).
[35]M. Cohen, Phys. Rev. **118**, 27 (1960).
[36]E. F. Talbot, H. R. Glyde, W. G. Stirling, and E. C. Svensson, Phys. Rev. B **38**, 11 229 (1988).
[37]J. A. Tarvin and L. Passell, Phys. Rev. B **19**, 1458 (1979).
[38]J. W. Halley and R. Hastings, Phys. Rev. B **15**, 1404 (1977).
[39]O. W. Dietrich, E. H. Graf, C. H. Huang, and L. Passell, Phys. Rev. A **5**, 1377 (1972).
[40]L. D. Landau and I. M. Khalatnikov, Zh. Eksp. Teor. Fiz. **19**, 637 (1949).
[41]F. Mezei, Phys. Rev. Lett. **44**, 1601 (1980).
[42]A. D. B. Woods and E. C. Svensson, Phys. Rev. Lett. **41**, 974 (1978).
[43]A. Griffin, Can. J. Phys. **65**, 1368 (1987).
[44]E. C. Svensson, W. G. Stirling, E. Talbot, and H. R. Glyde, Proceedings of the 18th International Conference on Low Temperature Physics, Kyoto, 1987 [Jpn. J. Appl. Phys. **26**, 33 (1987)].
[45]E. H. Graf, V. J. Minkiewicz, H. Bjerrum Møller, and L. Passell, Phys. Rev. A **10**, 1748 (1974).
[46]D. S. Greywall, Phys. Rev. B **21**, 1329 (1979).
[47]I. Waller and P. O. Fröman, Ark. Fys. **4**, 183 (1952).
[48]R. J. Donnelly, J. A. Donnelly, and R. N. Hills, J. Low Temp. Phys. **44**, 471 (1981).
[49]W. G. Stirling, Proceedings of the Second International Conference on Phonon Physics, edited by J. Kollár, M. Kroó, M. Menghárd, and T. Siklós (World Scientific, Singapore, 1985), p. 829, and private communication.